*Present address: Physics Department, Case Western Reserve University, Cleveland, Ohio 44106.
[1]D. J. Ernst, Ph.D. thesis, Massachusetts Institute of Technology, 1970 (unpublished).
[2]E. F. Redish and F. Villars, Ann. Phys. (N.Y.) 56, 355 (1970).
[3]H. Feshbach, Ann. Phys. (N.Y.) 5, 357 (1958); 19, 287 (1962).
[4]J. S. Bell and E. J. Squires, Phys. Rev. Letters 3, 96 (1959); J. S. Bell, in *Lectures on the Many Body Problem*, edited by E. R. Caianello (Academic, New York, 1962).
[5]F. Villars, in *Fundamentals in Nuclear Theory* (International Atomic Energy Agency, Vienna, 1967); N. Van-Giai, J. Sawicki, and N. Vinh Mau, Phys. Rev. 141, 913 (1966); N. Vinh Mau, in *Theory of Nuclear Structure* (International Atomic Energy Agency, Vienna, 1970).
[6]D. R. Thompson, I. Reichstein, W. McClure, and Y. C. Tang, Phys. Rev. 185, 1351 (1969), and references contained therein.
[7]D. A. Slanina and H. McManus, Nucl. Phys. A116, 271 (1968).
[8]This point and the effect of the inclusion of $W^{(-)}$ in optical potentials for heavier nuclei is presently being investigated.
[9]P. Nozieres, *Theory of Interacting Fermi Systems* (Benjamin, New York, 1964), p. 159.
[10]D. A. Zaikin, Nucl. Phys. A170, 584 (1971).

PHYSICAL REVIEW C VOLUME 6, NUMBER 5 NOVEMBER 1972

Distorted-Wave Theory of Deuteron Breakup*

Frank Rybicki†
University of Pittsburgh, Pittsburgh, Pennsylvania 15213, and University of Texas, Austin, Texas 78712

and

N. Austern
University of Pittsburgh, Pittsburgh, Pennsylvania 15213

(Received 26 July 1972)

Deuteron-breakup coincidence cross sections are calculated in the prior-interaction formulation of distorted-wave Born approximation (DWBA); both nuclear and Coulomb interactions are included. The results disagree with experiment. This is attributed to incorrect treatment of Coulomb distortion in the prior form of the outgoing wave function. Nuclear contributions to breakup are found to be as important as Coulomb contributions. Numerical procedures are developed that can also be used to include Coulomb excitation in DWBA calculations of inelastic scattering.

1. INTRODUCTION

The breakup of deuterons by collisions with nuclei has received extensive experimental study[1-3] in recent years by coincidence observations of neutrons and protons of definite momenta. Earlier experiments[4] studied only the low-energy proton backgound produced in deuteron-induced reactions.

It is generally believed that the breakup can be attributed to interaction of the individual neutron and proton of the deuteron with the average Coulomb and nuclear fields of the nucleus. The earliest theories of deuteron breakup[5] treat it in analogy to theories of photodisintegration; they take the point of view that the process is caused by the Coulomb field, which is treated as a perturbation. More accurate theories that still treat only the Coulomb field use Coulomb wave functions.[6,7] Theories of diffractive breakup have also been developed.[8] However, these theories are applicable only for very high deuteron energies.

The theory given in the present paper is developed in the spirit of direct-reaction theories that use distorted-wave Born approximation (DWBA). The formulation resembles that of Ref. 7; however, both the Coulomb and nuclear interactions are carried consistently, not only as transition operators but as distorting potentials.

The basic formulation of the theory[9] is given in Sec. 2. Detailed methods of calculation are discussed in Sec. 3; methods given there for handling the long-range tail of the Coulomb interaction can also be applied to DWBA calculations of inelastic scattering in which Coulomb excitation cannot be neglected. Further details of these methods appear in the Appendix.

Numerical calculations and comparisons with experiment[2,10] for 12- and 17-MeV deuterons on gold and 12-MeV deuterons on rhodium are given

in Secs. 4 and 5. The results are seen to be very poor. Reasons for the poor results and methods for improvement are discussed in Sec. 5. The oft-used notion of a well-defined "breakup radius" is also discussed there and is shown to be unreasonable.[2,3] Section 6 is a summary. Further details can be found in the work of Rybicki.[11]

2. THEORY

In our model the Hamiltonian that governs the target-plus-deuteron system is approximated by

$$H = T_n + U_n + T_p + U_p + V_p + V_{np}\,, \tag{2.1}$$

where T_n and T_p are kinetic energy operators, U_n and U_p are nuclear nucleon-nucleus interactions, V_p is the Coulomb proton-nucleus interaction, and V_{np} is the neutron-proton interaction. The interactions U_n and U_p are approximated by optical potentials. Although this choice is not the best effective interaction in a three-body model of the many-body deuteron-nucleus system,[12] it is a reasonable and simple approximation. Problems of the energy dependence of the optical potentials are resolved by choosing these potentials as if the neutron and proton have equal energy.

The cross section for breakup is[6,13,14]

$$\frac{d^3\sigma}{d\Omega_n d\Omega_p dE_p} = \frac{2m^3}{(2\pi)^5\hbar^6}\,\frac{k_n k_p}{K_i}\,|T|^2\,, \tag{2.2}$$

where m is the proton mass, $\hbar k_n$ and $\hbar k_p$ are the magnitudes of the neutron and proton momenta after breakup, $\hbar K_i$ is the deuteron momentum before breakup, and T is the transition amplitude. In DWBA, the transition amplitude can be expressed in two different ways,[15]

$$T^{(1)} = \langle \chi_p^{(-)}(\vec{k}_p, \vec{r}_p)\chi_n^{(-)}(\vec{k}_n, \vec{r}_n)\,|\,V_{np}(r)\,|\,\phi(r)\chi_d^{(+)}(\vec{K}_i, \vec{R})\rangle, \tag{2.3}$$

$$T^{(2)} = \langle \chi_d^{(-)}(\vec{K}_f, \vec{R})\phi^{(-)}(\vec{k}, \vec{r})\,|\,U_n(r_n) + U_p(r_p) + V_p(r_p)\,|\,\phi(r)\chi_d^{(+)}(\vec{k}_i, \vec{R})\rangle, \tag{2.4}$$

where $\chi_p^{(-)}$ and $\chi_n^{(-)}$ are optical-model wave functions with incoming wave boundary conditions, calculated in the potentials $U_p + V_p$ and U_n, respectively, $\phi^{(-)}$ is the neutron-proton scattering wave function with incoming wave boundary conditions, calculated in the potential V_{np}, $\chi_d^{(-)}$ and $\chi_d^{(+)}$ are deuteron optical-model wave functions with incoming and outgoing wave boundary conditions, respectively. In Eq. (2.4), the optical potential $U_d(R) + V_d(R)$, that is used to calculate $\chi_d^{(-)}(\vec{K}_f, \vec{R})$, does not appear as a transition operator. If this operator is included, the integrals over $\vec{r}$ and $\vec{R}$ decouple and the orthogonality of $\phi^{(-)}$ and ϕ makes the integral over $\vec{r}$ equal to zero. Thus, the interaction $U_d + V_d$ makes no contribution to the matrix element in Eq. (2.4).

The amplitude $T^{(2)}$, Eq. (2.4), is the one calculated here, since it is much more tractable than $T^{(1)}$ of Eq. (2.3). The integrand in $T^{(1)}$ is oscillatory for large r_n and r_p; there is nothing in the integrand to provide an upper cutoff to the integration. Partial wave decomposition of the wave functions in the integrand of $T^{(1)}$ does result in well-defined integrals.[13] However, this decomposition has difficulties: (1) The integrals are very difficult to calculate, since the integrands do not contain a damping factor; (2) the sum over partial waves converges very slowly. In the case of $T^{(2)}$, Eq. (2.4), the optical-model interactions provide the damping factor. The Coulomb interaction provides numerical complications, which can, however, be solved by known means. Thus, from a computational point of view, one chooses to calculate $T^{(2)}$ and not $T^{(1)}$. Hereafter, the superscript will be dropped from $T^{(2)}$. Another initial simplification will be omission of the spin-orbit parts of the nucleon-nucleus optical potentials. The most interesting feature of including the spin-orbit potentials would be their ability to excite the ^1S state of the unbound deuteron[16]; however, since only the difference between the spin-orbit potentials for neutrons and protons can couple the ^3S state to the ^1S unbound state, the contribution of this excitation to the transition amplitude would be small.

The bound deuteron is assumed to be in a pure ^3S state and it is represented by the Hulthén wave function,[17]

$$\phi(r) = \frac{N}{\sqrt{4\pi}}\,\frac{e^{-\alpha r} - e^{-\beta r}}{r}\,. \tag{2.5}$$

The unbound-deuteron wave function is represented by the scattering wave function,

$$\phi^{(+)}(\vec{k}, \vec{r}) = 4\pi \sum_{l,m} i^l \phi_l(k, r) Y_l^m(\hat{k}) Y_l^{m*}(\hat{r})\,, \tag{2.6}$$

where

$$\phi_0(k, r) = (kr)^{-1} e^{i\delta} \sin\delta \times (\cot\delta \sin kr + \cos kr - e^{-\xi r})\,, \tag{2.7}$$

$$\phi_{l\neq 0}(k, r) = j_l(kr)\,. \tag{2.8}$$

The phase shift δ in Eq. (2.7) is obtained from effective range theory.[17] The parameter ξ in Eq.

(2.7) is obtained by requiring that $\phi_0(k, r)$ be orthogonal to $\phi(r)$.[18]

In summary, the theory presented here can be thought of as a theory of inelastic scattering which utilizes the DWBA, but instead of exciting the target nucleus, the incident deuteron is excited into an unbound state.

3. METHOD OF CALCULATION

Since the amplitude is calculated in the DWBA, it is natural to write it as a form-factor sandwiched between optical-model wave functions. Since two mechanisms, nuclear and Coulomb, are being considered, it is desirable to split the amplitude into a nuclear part and a Coulomb part,

$$T = T^{(N)} + T^{(C)}. \tag{3.1}$$

The nuclear transition amplitude is

$$T^{(N)} = \langle \chi^{(-)}(\vec{K}_f, \vec{R}) | F^{(N)}(\vec{k}, \vec{R}) | \chi^{(+)}(\vec{K}_i, \vec{R}) \rangle, \tag{3.2}$$

and the Coulomb amplitude is

$$T^{(C)} = \langle \chi^{(-)}(\vec{K}_f, \vec{R}) | F^{(C)}(\vec{k}, \vec{R}) | \chi^{(+)}(\vec{K}_i, \vec{R}) \rangle. \tag{3.3}$$

The form factors in Eqs. (3.2) and (3.3) are defined by

$$F^{(N)}(\vec{k}, \vec{R}) \equiv \langle \phi^{(-)}(\vec{k}, \vec{r}) | U_n(r_n) + U_p(r_p) | \phi(r) \rangle, \tag{3.4}$$

$$F^{(C)}(\vec{k}, \vec{R}) \equiv \langle \phi^{(-)}(\vec{k}, \vec{r}) | V_p(r_p) | \phi(r) \rangle. \tag{3.5}$$

The brackets in Eqs. (3.4) and (3.5) imply integration over $\vec{r}$. The form factors, Eqs. (3.4) and (3.5), are expanded in multipoles,

$$F^{(x)}(\vec{k}, \vec{R}) = \sum_{l,m} i^{-l} Y_l^{m*}(\hat{R}) Y_l^m(\hat{k}) F_l^{(x)}(k, R); \tag{3.6}$$

here use of the superscript (x) means that the expression is valid for both the nuclear and the Coulomb form factors. The partial form factors, $F_l^{(x)}(k, R)$, can be expressed as one-dimensional integrals over the Fourier transforms of the potentials in Eqs. (3.4) and (3.5):

$$F_l^{(N)}(k, R) = 32\pi \int_0^\infty dq [X_p(q) + (-1)^l X_n(q)] \times j_l(qR) \Phi_l(k, q), \tag{3.7}$$

$$F_l^{(C)}(k, R) = 32\pi \int_0^\infty dq\, X_p^C(q) j_l(qR) \Phi_l(k, q), \tag{3.8}$$

where

$$X_p(q) = \int_0^\infty dr\, r \sin qr\, U_p(r), \tag{3.9}$$

$$X_n(q) = \int_0^\infty dr\, r \sin qr\, U_n(r), \tag{3.10}$$

$$X_p^C(q) = \int_0^\infty dr\, r \sin qr\, V_p(r), \tag{3.11}$$

j_l is the spherical Bessel function, and

$$\Phi_l(k, q) = q \int_0^\infty r^2 dr\, \phi_l(k, r) j_l(\tfrac{1}{2} qr) \phi(r). \tag{3.12}$$

The Coulomb form factor has a simple form for large R; it is obtained by putting the multipole expansion of the Coulomb potential into Eq. (3.5),

$$F_l^{(C)}(k, r) = A_l(k) R^{-(l+1)}, \tag{3.13}$$

where

$$A_l(k) = (4\pi)^2 (2l+1)^{-1} \int_0^\infty r^2 dr\, \phi_l(k, r) (\tfrac{1}{2} r)^l \phi(r). \tag{3.14}$$

The integrals in Eqs. (3.9) to (3.12) and (3.14) can be expressed in terms of elementary functions (see Appendix).

The nuclear and Coulomb transition amplitudes, Eqs. (3.2) and (3.3), are in the standard form of a DWBA amplitude.[19,20] The formulas below that describe the calculation of the transition amplitude T are the same or analogous to those of Refs. 19 and 20. The normalization is that of Ref. 19.

Both the nuclear and the Coulomb transition amplitudes, Eqs. (3.2) and (3.3), can be expressed as sums of standard multipoles,

$$T^{(x)} = \sum_l T_l^{(x)}, \tag{3.15}$$

where

$$T_l^{(x)} = [4\pi(2l+1)]^{1/2} K_f^{-2} \sum_m Y_l^m(\hat{k}) \beta^{(x) lm} \tag{3.16}$$

is the contribution of the lth-order multipole. The quantities $\beta^{(x) lm}$ are the DWBA matrix elements,[19]

$$\beta^{(x) lm} = \sum_{L_f L_i} \Gamma^{lm}_{L_f L_i} f^{(x) l}_{L_f L_i} P^m_{L_f}(\cos\theta_{K_f}), \tag{3.17}$$

where

$$\Gamma^{lm}_{L_f L_i} \equiv i^{L_i - L_f - l} (2L_f + 1) \left[\frac{(L_f - m)!}{(L_f + m)!} \right]^{1/2} \times \langle L_f l 00 | L_i 0 \rangle \langle L_f l m - m | L_i 0 \rangle \tag{3.18}$$

and

$$f^{(x) l}_{L_f L_i} = \frac{K_f}{K_i} \int_0^\infty dR\, \chi_{L_f}(K_f, R) F_l^{(x)}(k, R) \chi_{L_i}(K_i, R) \tag{3.19}$$

are the radial integrals.[19]

The nuclear radial integrals, Eq. (3.19), are computed by numerical integration in code JULIE.[19] Since the nuclear form factors decrease exponentially with increasing R, the integration can be cut

off at some maximum value of R. Also, there exist moderate values of L_f and L_i above which $f^{(N)l}_{L_fL_i}$ do not contribute to $\beta^{(N)lm}$.

The $l=0$ partial Coulomb form factor also decreases exponentially with increasing R; thus it is in the same category as the nuclear form factors and is easily handled. However, for $l\neq 0$ the partial Coulomb form factors fall off like inverse powers of R, Eq. (3.13). This behavior of the tail has two consequences. First, the integral in Eq. (3.19) converges slowly; numerical integration will not be accurate. Second, the sum in Eq. (3.17) converges slowly; therefore, the radial integrals in Eq. (3.17) that have large values of L_f and L_i must be obtained by a method that is more efficient than numerical integration.

The Coulomb form factors for $l\neq 0$ are handled by a procedure pictured by the diagram in Fig. 1. The diagram is a graph of R vs L, where L is some average of L_f and L_i. The R-L space is divided into three regions, a different method of evaluating the radial integral is used in each region. In region 1, the optical functions and the form factors are known numerically; numerical integration gives good values for their overlap in the region $0<R<\tilde{R}$.

Region 2 in Fig. 1 extends the radial integrations for the low partial waves; it gives nonnegligible contributions to their overlap. In region 2, the form factor is given by Eq. (3.13) and the optical-model wave functions are given by their asymptotic representation,[19,20]

$$\chi_L(K,R)\sim e^{i\sigma_L}\tfrac{1}{2}i\,[H^*_L(KR)-\eta_L H_L(KR)]\,, \qquad (3.20)$$

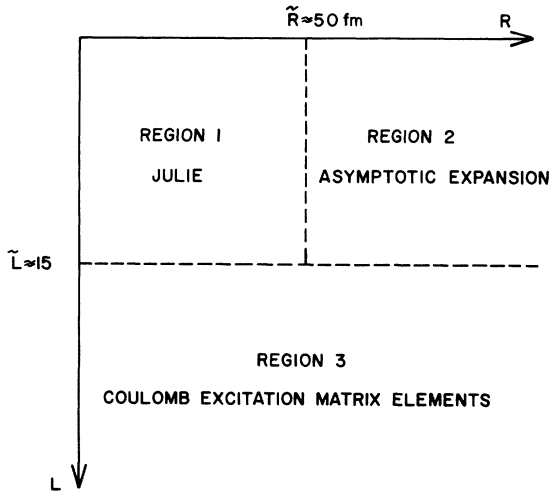

FIG. 1. Graphical display of the methods used to calculate the Coulomb radial integrals, $f^{(C)l}_{L_fL_i}$. The method used depends on the radius R and on the average partial wave L.

where σ_L is the Coulomb phase shift, η_L is the reflection coefficient, and

$$H_L=G_L+iF_L \qquad (3.21)$$

is the Coulomb wave functions with outgoing waves. The functions F_L and G_L are the regular and irregular Coulomb wave functions, respectively. Thus for $L\lesssim\tilde{L}$, the radial integral is expressed as two terms,

$$\begin{aligned} f^{(C)l}_{L_fL_i}=&\frac{K_f}{K_i}\int_0^{\tilde{R}}dR\,\chi_{L_f}(K_f,R)F^{(C)}_l(k,R)\chi_{L_i}(K_i,R)\\ &-\frac{1}{4}\frac{K_f}{K_i}e^{i(\sigma_{L_f}+\sigma_{L_i})}A_l(k)\\ &\times\int_{\tilde{R}}^{\infty}dR[H^*_{L_f}(K_fR)-\eta_{L_f}H_{L_f}(K_fR)]R^{-(l+1)}\\ &\times[H^*_{L_i}(K_iR)-\eta_{L_i}H_{L_i}(K_iR)]\,. \end{aligned} \qquad (3.22)$$

The first term contains the integral across region 1 that is done numerically; the second term contains the integral across region 2 that is done analytically. To evaluate the integral in region 2 the Coulomb wave function is represented by its asymptotic series,[21]

$$H_L(\rho)\sim e^{i\theta_L(\rho)}\sum_{\mu=0}^{\infty}a^L_\mu\rho^{-\mu}, \qquad (3.23)$$

where

$$\rho=KR\,,$$

$$\theta_L(\rho)=\rho-(n\ln 2\rho)-(L\pi/2)+\sigma_L\,, \qquad (3.24)$$

$$a^L_{\mu+1}=\{n(2\mu+1)+i[n^2+L(L+1)-\mu(\mu+1)]\}a^L_\mu/2(\mu+1)\,, \qquad (3.25)$$

$$a^L_0=1\,.$$

The accuracy to which the asymptotic series represents the function is less than the first term not used; the product of two asymptotic series is again an asymptotic series.[22] The integral in region 2 contains four terms; there are two distinct kinds of integrals, the other two are related by complex conjugation. Denote the two distinct integrals by

$$I^{(1)l}_{L_bL_a}\equiv\int_{\tilde{R}}^{\infty}dR\,R^{-(l+1)}H_{L_b}(K_bR)H_{L_a}(K_aR) \qquad (3.26)$$

and

$$I^{(2)l}_{L_bL_a}\equiv\int_{\tilde{R}}^{\infty}dR\,R^{-(l+1)}H_{L_b}(K_bR)H^*_{L_a}(K_aR)\,. \qquad (3.27)$$

The integrals in Eqs. (3.26) and (3.27) are evaluated by inserting the asymptotic series, Eq. (3.23), into Eqs. (3.26) and (3.27) and by integrating term by term. The results are asymptotic

series,

$$I^{(1)l}_{L_b L_a} \sim \frac{i}{K_b + K_a} \tilde{R}^{-(l+1)} e^{i(\theta_{L_b} + \theta_{L_a})} \times \sum_{\nu=0}^{\infty} C^{(1)L_b L_a}_{\nu} \mathcal{J}^{\nu+l+1}[(K_b + K_a)\tilde{R}, (n_b + n_a)], \tag{3.28}$$

$$I^{(2)l}_{L_b L_a} \sim \frac{i}{K_b - K_a} \tilde{R}^{-(l+1)} e^{i(\theta_{L_b} - \theta_{L_a})} \times \sum_{\nu=0}^{\infty} C^{(2)L_b L_a}_{\nu} \mathcal{J}^{\nu+l+1}[(K_b - K_a)\tilde{R}, (n_b - n_a)], \tag{3.29}$$

where

$$C^{(1)L_b L_a}_{\nu} = \sum_{\mu=0}^{\nu} a^{L_b}_{\mu} a^{L_a}_{\nu-\mu}, \tag{3.30}$$

$$C^{(2)L_b L_a}_{\nu} = \sum_{\mu=0}^{\nu} a^{L_b}_{\mu} a^{L_a *}_{\nu-\mu}. \tag{3.31}$$

The function $\mathcal{J}$ is represented by an asymptotic series in inverse powers of the first argument,

$$\mathcal{J}^{\mu}(\alpha, n) \sim \sum_{\nu=0}^{\infty} \frac{\Gamma(\mu + \nu + in)}{(i\alpha)^{\nu} \Gamma(\mu + in)}, \tag{3.32}$$

where Γ is the gamma function.[21]

Consider Fig. 1 again. In region 3, the optical-model wave functions are just regular Coulomb wave functions,

$$\chi_L(K, R) \cong e^{i\sigma_L} F_L(KR). \tag{3.33}$$

For the large angular momenta that occur in region 3, the partial waves do not penetrate the centrifugal barrier, therefore these partial waves do not sample the nuclear potential and suffer only Coulomb scattering. Since the optical-model wave functions of large L are negligible at small values of R, Eq. (3.13) can be used for the form factor. Hence the radial integral can be written

$$f^{(C)l}_{L_f L_i} \cong \frac{K_f}{K_i} A_l(k) e^{i(\sigma_{L_f} + \sigma_{L_i})} \times \int_0^{\infty} dR\, F_{L_f}(K_f R) R^{-(l+1)} F_{L_i}(K_i R). \tag{3.34}$$

The integral in Eq. (3.34),

$$J^l_{L_f L_i} = \int_0^{\infty} dR\, F_{L_f}(K_f R) R^{-(l+1)} F_{L_i}(K_i R), \tag{3.35}$$

is known from the theory of Coulomb excitation,[23] it has an analytic solution in terms of elementary functions, gamma functions, and Appell functions.[23,24] For large L_f and L_i, the integral can be well approximated by the classical limit. In the limit as $|\tilde{L} + i\bar{n}| \to \infty$, it approaches,[23,24]

$$J^l_{L_f L_i} \to \tfrac{1}{4}(\bar{K}/\bar{n})^l \int_{-\infty}^{\infty} dx\, e^{i\xi[\epsilon \sinh(x) + x]} \times \frac{[\cosh(x) + \epsilon + i(\epsilon^2 - 1)^{1/2} \sinh(x)]^{\mu}}{[\epsilon \cosh(x) + 1]^{l+\mu}}, \tag{3.36}$$

where

$$\begin{aligned} \mu &= L_f - L_i, \\ \xi &= n_f - n_i, \\ \bar{L} &= \tfrac{1}{2}(L_f + L_i), \\ \bar{n} &= \tfrac{1}{2}(n_f + n_i), \\ \bar{K} &= \tfrac{1}{2}(K_f + K_i), \\ \epsilon &= \left[1 + \frac{\bar{L}(\bar{L}+1)}{\bar{n}^2}\right]^{1/2}. \end{aligned} \tag{3.37}$$

Equation (3.36) is a good approximation for $J^l_{L_f L_i}$ even for moderate values of $\bar{L}$.[23]

The criteria used to determine $\tilde{R}$ and $\tilde{L}$ in Fig. 1 are related. First, $\tilde{R}$ is chosen large enough so that the asymptotic expansions in Eqs. (3.28) and (3.29) give a good representation of the integrals in Eqs. (3.26) and (3.27). Once $\tilde{R}$ is determined, $\tilde{L}$ is determined. The reason for this is that for a fixed $\tilde{R}$ the asymptotic expansions are valid only for values of $L \lesssim \tilde{L}$. The relationship arises because $\tilde{L}$ must be large enough so that the form factor is well represented by Eq. (3.13) where the optical-model partial waves in region 3 have appreciable magnitude.

4. CALCULATIONS

Calculations were performed for a gold target with incident deuteron energies of 12 and 17 MeV and for a rhodium target with an incident deuteron energy of 12 MeV. The potential used for the deuteron optical-model wave functions has the form

$$U(r) = -Vf_{\mathrm{WS}}(x) - iWf_{\mathrm{WS}}(x') + iW' f_{\mathrm{DWS}}(x'), \tag{4.1}$$

where

$$\begin{aligned} f_{\mathrm{WS}}(x) &= (e^x + 1)^{-1}, \\ f_{\mathrm{DWS}}(x) &= \frac{d}{dx}(e^x + 1)^{-1}, \\ x &= \frac{r - r_0 A^{1/3}}{a}, \\ x' &= \frac{r - r_0' A^{1/3}}{a'}. \end{aligned}$$

The Coulomb interaction is represented by the

TABLE I. Deuteron optical-potential parameters, energies in MeV, lengths in 10^{-13} cm.

Target	V	r_0	a	r_c	W	W'	r'_0	a'
Au^{197}	105.5	1.15	0.81	1.15	0	69.1	1.38	0.68
Rh^{103}	96.05	1.15	0.81	1.3	20.12	0	1.242	0.778

Coulomb potential for a uniformly charged sphere with a radius of $r_c A^{1/3}$. The deuteron parameters are listed in Table I. For the gold calculation at 12 MeV the deuteron optical parameters are the Perey average[25] set for 12-MeV deuterons on gold. The same parameters were used for the 17-MeV calculation for the sake of simplicity in comparing to the 12-MeV calculation. The parameters used for the rhodium calculation are the best-fit parameters for 14.5-MeV deuteron elastic scattering on ^{100}Mo, given by Hjorth, Lin, and Johnson.[26] The parameters used for the proton and neutron optical-model potentials are listed in Table II; these are average Perey parameters.[27]

For both the 12- and the 17-MeV gold calculation, the multipoles of order $l=0$, 1, 2 for both the nuclear and Coulomb interactions were included. For 12 MeV, the relative momenta k $=0.126$, 0.130, 0.140, 0.150, 0.160, 0.180, 0.200 were used. For 17 MeV, the relative momenta $k=0.05$, 0.10, 0.15, 0.20, 0.25, 0.30, 0.35, 0.40 were used. For the calculation of 12-MeV deuterons on rhodium, the nuclear monopole, the Coulomb dipole, and both the nuclear and Coulomb quadrupole were included. The relative momenta $k=0.13$, 0.18, 0.277, 0.288 were used.

5. RESULTS AND DISCUSSION

Figure 2 shows the theoretical and experimental[12] proton energy spectra for a gold target with E_d $=12$ MeV, $\theta_n=20°$, and $\theta_p=50°$. The predicted spectrum disagrees with experiment; the energies at which the peaks occur differ by 3.7 MeV and the magnitudes at the peaks differ by a factor of 16.5. Also, the theoretical spectrum peaks at an energy 1.9 MeV below half the total energy of the two outgoing particles. From physical considerations it is more likely for the proton to have more than half the available energy, because the proton is accelerated by the Coulomb potential as it leaves the region of breakup.

TABLE II. Nucleon-nucleus optical-potential parameters, as in Table I.

Target	Projectile	V	r_0	a	r_c	W	W'	r'_0	a'
Au^{197}	Proton	58	1.25	0.65	1.25	0	40	1.25	0.45
Au^{197}	Neutron	42	1.25	0.65	···	0	40	1.25	0.45
Rh^{103}	Proton	57	1.25	0.65	1.25	0	0	···	···
Rh^{103}	Neutron	47	1.25	0.65	···	0	0	···	···

One can gain some understanding of the discrepancy between theory and experiment by examining the final-state wave function in the matrix element in Eq. (2.4). The final state contains a deuteron optical-model wave function; this implies that the Coulomb interaction in the final state acts on the center of mass of the outgoing particles, whereas in reality it should act only on the proton. Therefore the structure of Eq. (2.4) has the consequence that after breakup both the neutron and proton are accelerated, rather than just the proton. This effect tends to upset the division of energies. The magnitude of the cross section is affected in a similar fashion: The deuteron center-of-mass wave function is severely damped by the Coulomb barrier, whereas the proton alone would experience a smaller barrier.

To investigate further the way the DWBA model treats the Coulomb effects just described, two additional calculations were performed in which the final-state Coulomb effects were expected to have less importance. One, for 17-MeV deuterons on gold involves raising the incident energy, the other, for 12-MeV deuterons on rhodium involves a decrease of the target nucleus charge.

Table III presents the results of the calculations

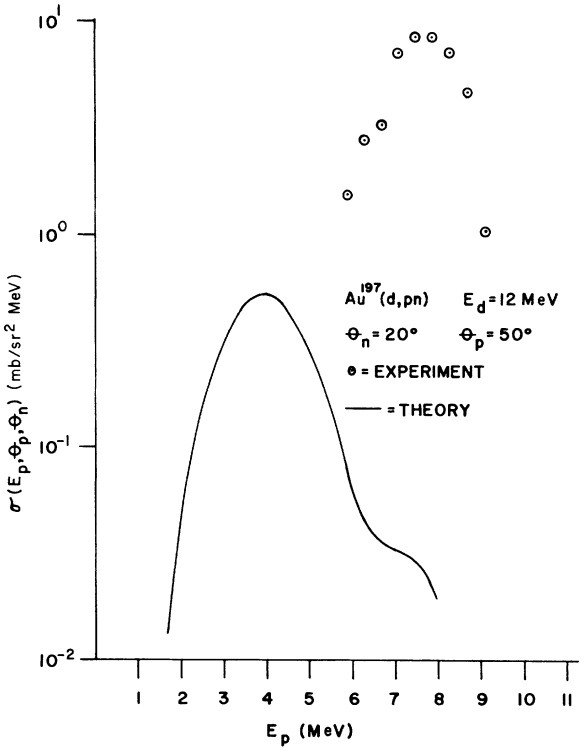

FIG. 2. Comparison of the theoretical and experimental proton energy spectra, $\sigma(E_p,\theta_p,\theta_n)$, for $Au^{197}(d,pn)$ with $E_d=12$ MeV, $\theta_p=50°$, and $\theta_n=20°$.

TABLE III. Calculated proton spectrum for Au^{197}-(d,pn) with $E_d = 17$ MeV, $\theta_n = 20°$, and $\theta_p = 50°$. Energies in MeV, cross sections in mb/sr^2 MeV.

E_p	$\sigma(E_p, \theta_p, \theta_n)$
3.93	1.965
5.02	2.656
9.45	6.538
10.54	3.587

for gold at 17 MeV, with $\theta_n = 20°$ and $\theta_p = 50°$. Compared with the 12-MeV calculation, the 17-MeV cross section is 10 times larger and the energy sharing between neutron and proton is more nearly as expected.

Columns 1–6 in Table IV give the results of the 12-MeV rhodium calculation. Column 8 gives experimental cross sections[2] integrated over proton energy. For $\theta_p = 30°$ and 50° there is good qualitative agreement. For $\theta_p = -50°$ the theoretical cross section is small by a factor ~20. The energy sharing is more nearly as expected, with a larger cross section for protons that have more than half the available energy.

The improved results obtained in the two calculations that have reduced Coulomb effect support the previous claim that the discrepancies in the 12-MeV gold calculation are caused by an incorrect treatment of the Coulomb barriers in the exit channel.

Coulomb-nuclear interference can be discussed to some extent in terms of symmetries of the DWBA matrix element. We see in Eq. (2.4) that in the prior form of this matrix element, the starting point of the present article, the only difference between the roles of the neutron and proton is the direction of $\vec{k}$, the relative momentum. It is interesting that the Coulomb and nuclear contributions in the transition amplitude behave very differently with respect to changes of the sign of $\vec{k}$. The Coulomb contribution to the transition amplitude comes predominantly from the dipole term. The monopole term is suppressed by the orthogonality of the bound and continuum deuteron wave functions. The quadrupole and higher-order multipoles make decreasing contributions to T; in other words, the multipole series converges. (The convergence of the series is seen by considering the overlap of the bound-state wave function with a particular partial wave in the expansion of the unbound deuteron wave function; the higher the partial wave the poorer is the overlap with the bound state if $|\vec{k}|$ is not too large.) For the nuclear interaction the even multipoles are more significant than the odd multipoles. Eq. (3.7) shows that only the difference between the proton-nucleus and the neutron-nucleus interactions contributes to the odd multipoles, therefore these are strongly suppressed. The contribution of the monopole term is reduced somewhat by the orthogonality of the deuteron relative wave functions. However, the reduction is not as severe as in the Coulomb case, because the nuclear potential changes magnitude fairly rapidly as a function of radius in the region of the nuclear surface. Thus, the dominant multipoles for the nuclear interaction are the monopole and the quadrupole. Under these conditions we see that if either the Coulomb or nuclear contribution to the breakup were to dominate over the other, $T(\vec{k}, \vec{K}_f)$ would be symmetric under the transformation $\vec{k} \to -\vec{k}$. The lack of this symmetry in the transition amplitude is a measure of interference between the Coulomb and nuclear contributions.

Another kind of Coulomb-nuclear interference manifests itself in the distorted waves for the motion of the deuteron center of mass, in that both interactions give rise to the distortions in these wave functions. Interference of this type does not affect the symmetry of $T(\vec{k}, \vec{K}_f)$.

As an example of interference between Coulomb and nuclear breakup, Figure 3 displays $|T|^2$ as a function of θ_{K_f}. The target is gold with $E_d = 17$ MeV and $k = 0.1$; the direction of $\vec{k}$ is chosen so that $|T|^2$ is a maximum. The graph of $|T|^2$ for $-\vec{k}$ is also plotted. The angular distributions are out of phase; this is indicative of interference between the nuclear and the Coulomb amplitudes.

Detailed studies of the contributions of the various multipoles in our numerical calculations are given in Ref. 11. A brief review of the remarks

TABLE IV. Comparison of theory and experiment for $Rh^{103}(d,pn)$ with $E_d = 12$ MeV and $\theta_n = 20°$. Columns 1–6 show theoretical proton energy spectra for $\theta_p = 50$, 30, and −50°, respectively. Column 8 shows the experimental cross section, $\sigma(\theta_n, \theta_p)$, from Ref. 2. Units as in Table III.

$\theta_p = 50°$		$\theta_p = 30°$		$\theta_p = -50°$			
E_p	$\sigma(E_p, \theta_p, \theta_n)$	E_p	$\sigma(E_p, \theta_p, \theta_n)$	E_p	$\sigma(E_p, \theta_p, \theta_n)$	θ_p	$\sigma(\theta_p, \theta_n)$
2.04	0.616	1.46	1.821	1.82	0.059	50°	5
3.80	1.654	2.32	3.511	3.22	0.120	30°	12
5.57	5.600	7.05	12.956	6.20	0.241	−50°	5.5
7.35	3.757	7.93	4.782	7.61	0.131		

in Ref. 11 follows: The nuclear and Coulomb amplitudes, Eq. (3.15), are of the same order of magnitude. The dipole contribution dominates the Coulomb amplitude; the monopole term is indeed negligible, as was argued from the notion of wavefunction orthogonality. For the nuclear amplitude, the monopole and quadrupole terms contribute about equally and the dipole term is negligible. Therefore, in the transformation $\vec{k}$ to $-\vec{k}$, the magnitudes of the nuclear and Coulomb amplitudes barely change, but the sign of the Coulomb amplitude reverses. Therefore a peak in the distribution for $\vec{k}$ corresponds to a minimum in the distribution for $-\vec{k}$ and vice versa.

A very good example of symmetry under the transformation $\vec{k} \rightarrow -\vec{k}$ was found in a calculation for 17-MeV deuterons on gold with $k = 0.4$. The nuclear quadrupole dominates the amplitude in this case. It can be seen that symmetry with respect to the sign of $\vec{k}$ is equivalent to symmetry in the energy sharing between the neutron and proton, if their momenta are perpendicular. Just this symmetry is seen in the calculated curve in Fig. 4 derived from the $k = 0.4$ results. Unfortunately, the corresponding experimental spectrum does not have a peak for low proton energy, another example of our incorrect treatment of Coulomb effects.

It has been customary in experimental articles[2,3] to use the unsymmetrical energy sharing between the neutron and proton as evidence for a most probable radius at which breakup occurs. This "breakup radius" is often thought to be fairly large It is most convenient to study the breakup radius theoretically by examining the distribution of angular momenta[20] that contribute to the breakup amplitude. Let us define a quantity $\alpha_{L_f}^{(x)lm}$, such that the amplitude of Eq. (3.17) is

$$\beta^{(x)lm} = \sum_{L_f} \alpha_{L_f}^{(x)lm} Y_{L_f}^{m}(\hat{K}_f) . \tag{6.1}$$

The explicit expression for $\alpha_{L_f}^{(x)l}$ then is

$$\alpha_{L_f}^{(x)lm} = (-)^m \left(\frac{4\pi}{2L_f+1}\right)^{1/2} \left(\frac{(L_f+m)!}{(L_f-m)!}\right)^{1/2} \times \sum_{L_i} \Gamma_{L_f L_i}^{lm} f_{L_f L_i}^{(x)l} , \tag{6.2}$$

where $\Gamma_{L_f L_i}^{lm}$ is given by Eq. (3.18) and $f_{L_f L_i}^{(x)l}$ is given by Eq. (3.19). Figs. 5 and 6 show the magnitudes of $\alpha_{L_f}^{(x)lm}$ for the nuclear and Coulomb contributions, respectively. The target is gold, the incident deuteron energy is 12 MeV, and the relative momentum, $k = 0.13$. This value for the relative momentum corresponds to the peak in the theoretical proton energy spectrum, Fig. 2. Looking at Fig. 5, one sees that there is no one dominant partial wave for the nuclear breakup. Angular momenta from 2 to 8 contribute significantly. We note that in the expression for the transition amplitude, Eq. (3.16), the β^{lm}'s are weighted by a factor of $(2l+1)^{1/2}$. For the Coulomb contribution to the breakup, Fig. 6, there is no localization at all. The magnitude of $\alpha_{L_f}^{(c)lm}$ for $L_f = 25$ is di-

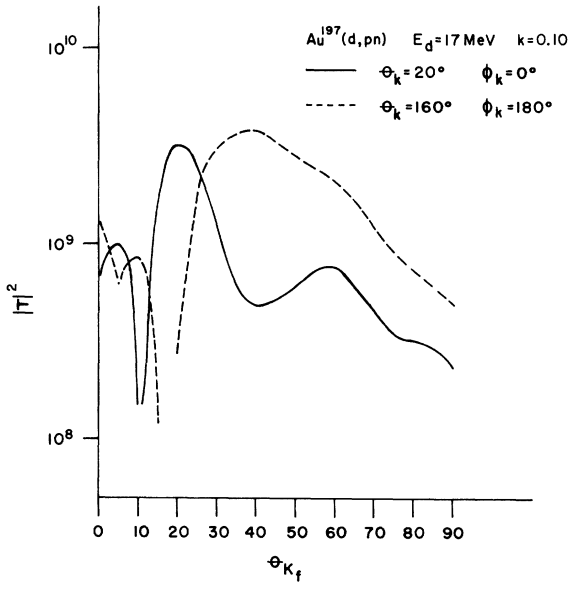

FIG. 3. Angular distribution of $|T|^2$, the absolute square of the transition amplitude, as a function of θ_{K_f}, the angle between the unbound deuteron center-of-mass momentum and the incident deuteron momentum. The reaction is $Au^{197}(d, pn)$ with $E = 17$ MeV. The two curves correspond to the two unbound deuteron relative momenta $\vec{k}$ and $-\vec{k}$, where $\vec{k}$ is specified by $k = 0.1$, $\theta_k = 20°$, and $\phi_k = 0°$.

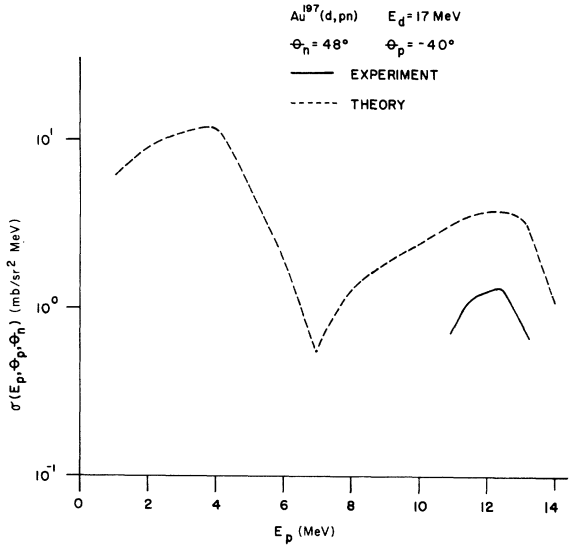

FIG. 4. Same as Fig. 2, except that $E_d = 17$ MeV, $\theta_p = -40°$, and $\theta_n = 48°$.

minished by only a factor of ~10 from the maximum value, which occurs at $L_f \approx 6$. Thus from the point of view of angular momentum localization, there is no well-defined region of space in which the breakup reaction takes place.

6. SUMMARY

We see that breakup cross sections calculated with the prior DWBA amplitude disagree with experiment, apparently because the Coulomb potential affects the center-of-mass coordinate of the outgoing particles instead of the proton coordinate. Despite this defect of the calculations we are able to conclude that nuclear interactions contribute as strongly to breakup as the Coulomb interaction, even for 12-MeV deuterons incident on a high-Z target nucleus such as gold, contrary to former belief.

We see that the breakup does not occur in the vicinity of any particular characteristic radius, despite frequent use of that concept.

The numerical procedures used here to include Coulomb excitation can be generalized for use in any DWBA calculation of inelastic scattering.

Finally, we note the inherent defects of a theoretical model based on average Coulomb and nuclear potentials: Such a model neglects internal coordinates of the target nucleus. Recent measurements of breakup cross sections show resonances and rapid variations with mass number,[3] effects that cannot be produced by a potential model. The existence of these effects is in good accord with the importance found for nuclear interactions in the present calculations. Of course, the potential model retains its interest, despite resonance effects, because it is expected to describe the average amplitude on which the resonances sit. For this reason more accurate calculations with the potential model should help provide further understanding of the importance of the resonance effects.

Improved DWBA calculations in the potential model are underway, using the post form of the amplitude, Eq. (2.3). The poor convergence of the numerical integrations in this amplitude is handled by the method of contour integration in the complex radius plane.[28]

Note added in proof: Meanwhile, calculations using the post form of the transition amplitude have been performed by Lang, Balzer, Jarczyk, Müller, and Marmier and by Baur and Trautmann. Encouraging agreement with experiment is found.

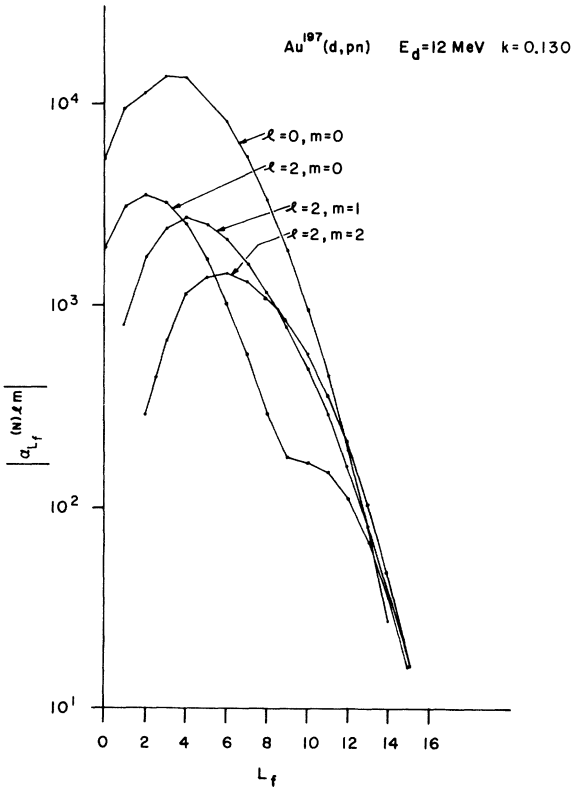

FIG. 5. Contributions to the nuclear amplitude, $\beta^{(N)lm}$, for the L_f partial wave in the final-state deuteron optical-model wave function. The reaction is $Au^{197}(d, pn)$ with $E_d = 12$ MeV and $k = 0.130$ fm^{-1}.

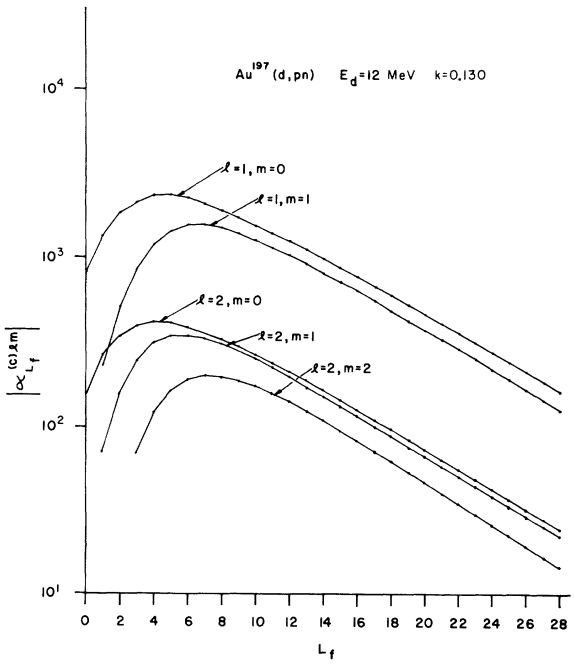

FIG. 6. Same as Fig. 5, except that the contributions are to the Coulomb amplitude, $\beta^{(C)lm}$.

ACKNOWLEDGMENTS

Dr. R. C. Johnson initially pointed out the good convergence properties of the prior DWBA amplitude. We wish to express our appreciation to Professor Richard M. Drisko for many helpful discussions, for his permission to use his DWBA code JULIE, and for his aid in making some of the calculations at the Oak Ridge National Laboratory. One of us (FR) would like to thank Dr. Robert H. Bassel for some helpful discussions. We are grateful to Professor B. L. Cohen and Dr. C. Fink for providing us with experimental data before publications. Finally, the cooperation of the University of Pittsburgh Computer Center and C. O'Toole in particular is appreciated.

APPENDIX

The Fourier transforms for the terms in the optical potential, Eq. (4.1), are:

$$f_{\mathrm{WS}}(q)=\left\{\pi a\,\mathrm{csch}(\pi aq)\times[\pi a\,\mathrm{ctnh}(\pi aq)\sin(q\tilde{r})-\tilde{r}\cos(q\tilde{r})]-2a^3q\sum_{n=1}^{\infty}(-)^n\frac{n}{(n^2+a^2q^2)^2}\,e^{-n\tilde{r}/a}\right\},\tag{A1}$$

$$f_{\mathrm{DWS}}(q)=\left\{\pi a^2\,\mathrm{csch}(\pi aq)\times[\{1-\pi aq\,\mathrm{ctnh}(\pi aq)\}\cos(q\tilde{r})-q\tilde{r}\sin(q\tilde{r})]-2a^3q\sum_{n=1}^{\infty}(-)^n\frac{n^2}{(n^2+a^2q^2)^2}\,e^{-n\tilde{r}/a}\right\},\tag{A2}$$

where $\tilde{r}=r_0A^{1/3}$. The Fourier transform for the Coulomb potential is

$$X_p^C(q)=\frac{3Ze^2}{q^2\tilde{r}}\,j_1(q\tilde{r}),\tag{A3}$$

where $\tilde{r}=r_{oc}A^{1/3}$, and j_1 is the spherical Bessel function.

The integral in Eq. (3.12) is expressed in terms of elementary functions as

$$\begin{aligned}\Phi_0(k,q)=\frac{Ne^{i\delta}\sin(\delta)}{k\sqrt{4\pi}}\Bigg\{&\tfrac{1}{2}\cot(\delta)\ln\left[\frac{\alpha^2+(k+\frac{1}{2}q)^2}{\alpha^2+(k-\frac{1}{2}q)^2}\right]\\&+\tan^{-1}\left(\frac{k+\frac{1}{2}q}{\alpha}\right)-\tan^{-1}\left(\frac{k-\frac{1}{2}q}{\alpha}\right)-\tfrac{1}{2}\cot(\delta)\ln\left[\frac{\beta^2+(k+\frac{1}{2}q)^2}{\beta^2+(k-\frac{1}{2}q)^2}\right]\\&-\tan^{-1}\left(\frac{k+\frac{1}{2}q}{\beta}\right)+\tan^{-1}\left(\frac{k-\frac{1}{2}q}{\beta}\right)-2\tan^{-1}\left(\frac{\frac{1}{2}q}{\alpha+\xi}\right)+2\tan^{-1}\left(\frac{\frac{1}{2}q}{\beta+\xi}\right)\Bigg\},\end{aligned}\tag{A4}$$

$$\Phi_{l\neq0}(k,q)=\frac{N}{k\sqrt{4\pi}}\left\{Q_l\left(\frac{\alpha^2+k^2+(\frac{1}{2}q)^2}{kq}\right)-Q_l\left(\frac{\beta^2+k^2+(\frac{1}{2}q)^2}{kq}\right)\right\}.\tag{A5}$$

The parameters N, α, β, δ, and ξ are from Eqs. (2.5) and (2.7). Q_l is the Legendre function of the second kind[21]; $Q_l(x)$ has a pole at $x=1$; but, it is analytic for $x>1$. The arguments of Q_l in Eq. (A5) are always greater than one. Eqs. (A4) and (A5) are not defined at $k=0$; for this special case the integrals are

$$\Phi_0(k=0,q)=\frac{2Na}{\sqrt{4\pi}}\left\{\tan^{-1}\left(\frac{\frac{1}{2}q}{\alpha}\right)-\tan^{-1}\left(\frac{\frac{1}{2}q}{\beta}\right)-\frac{1}{a}\left[\frac{\frac{1}{2}q}{\alpha^2+(\frac{1}{2}q)^2}-\frac{\frac{1}{2}q}{\beta^2+(\frac{1}{2}q)^2}\right]-\tan^{-1}\left(\frac{\frac{1}{2}q}{\alpha+\xi}\right)+\tan^{-1}\left(\frac{\frac{1}{2}q}{\beta+\xi}\right)\right\},\tag{A6}$$

$$\Phi_{l\neq0}(k=0,q)=0.\tag{A7}$$

The quantity a in Eq. (A6) is the neutron-proton triplet scattering length, defined by $ka=-\tan\delta$, where δ is the triplet s-wave phase shift.

Finally, we give the result of the integration in Eq. (3.14):

$$A_l(k)=32\pi^2(2l+1)^{-1}2^{-(l+1)}(2k)^l\,l\,![(\alpha^2+k^2)^{-(l+1)}-(\beta^2+k^2)^{-(l+1)}].\tag{A8}$$

*Work supported by the National Science Foundation and partly by the U. S. Atomic Energy Commission.

†Present address: Temple University, Philadelphia, Pennsylvania 19122.

[1]F. Udo and L. A. Ch. Koerts, Nucl. Phys. 70, 145 (1965); F. Udo, Rev. Mod. Phys. 37, 365 (1965); A. Pollitzer, W. Wölfli, J. Lang, R. Müller, and P. Marmier, Helv. Phys. Acta. 41, 439 (1968).

[2]E. C. May, B. L. Cohen, and T. M. O'Keffe, Phys. Rev. 164, 1253 (1967).

[3]O. F. Nemets, V. M. Pugach, M. V. Sokolov, and B. G. Struzhko, in Proceedings of the International Symposium on Nuclear Structure, Dubna, USSR, 1968 (unpublished); C. L. Fink, B. L. Cohen, J. C. van der Weerd, and R. J. Petty, Phys. Rev. 185, 1568 (1969).

[4]E. W. Hamburger, B. L. Cohen, and R. E. Price, Phys. Rev. 121, 1143 (1961), and references therein.

[5]J. R. Oppenheimer, Phys. Rev. 47, 845 (1935); S. M Dancoff, *ibid.* 72, 1017 (1947).

[6]L. Landau and E. Lifshitz, Zh. Eksperim, i Teor. Fiz. 18, 750 (1948); H. B. Ketchum, M.S. dissertation, University of Pittsburgh, 1961 (unpublished).

[7]C. J. Mullin and E. Guth, Phys. Rev. 82, 141 (1951); R. Gold and C. Wong, Phys. Rev. 132, 2586 (1963).

[8]R. J. Glauber, Phys. Rev. 99, 1515 (1955); A. I. Akhieser and A. G. Sitenko, *ibid.* 106, 1236 (1957); A. G. Sitenko and V. K. Tartakovsky, Nucl. Phys. 13, 420 (1959); I. I. Ivanchick and V. S. Popov, Zh. Eksperim. i Teor. Fiz. 36, 499 (1959) [transl.: Soviet Phys.–JETP 9, 347 (1959)]; A. G. Sitenko, Yu. A. Berezhnoi, and M. V. Evlanov, Ukr. Fiz. Zh. 13, 804 (1968) [transl.: Ukr. Phys. J. 13, 570 (1968)].

[9]R. C. Johnson, private communication.

[10]B. L. Cohen and C. Fink, private communication.

[11]F. Rybicki, Ph.D. thesis, University of Pittsburgh, 1970 (unpublished).

[12]N. Austern and K. C. Richards, Ann. Phys. (N.Y.) 49, 309 (1968).

[13]E. B. Levshin, Izv. Akad. Nauk SSSR, Ser. Fiz. 30, 367 (1966) [transl.: Bull. Acad. Sci. USSR, Phys. Ser. 30, 372 (1966)].

[14]N. Austern, *Direct Nuclear Reaction Theories* (Wiley-Interscience, New York, 1970).

[15]E. M. Henley and C. E. Lacy, Phys. Rev. 160, 835 (1967).

[16]J. V. Noble, Phys. Rev. 162, 934 (1967).

[17]L. Hulthén and M. Sugawara, in *Encyclopedia of Physics*, edited by S. Flügge (Springer-Verlag, Berlin, 1957), Vol. 39; R. Wilson, *The Nucleon-nucleon Interaction* (Interscience, New York, 1963).

[18]N. Austern, Nucl. Phys. 7, 195 (1958).

[19]R. H. Bassel, R. M. Drisko, and G. R. Satchler, Oak Ridge National Laboratory Report No. ORNL-3240 (unpublished).

[20]G. R. Satchler, *Lectures in Theoretical Physics* (Univ. of Colorado Press, Boulder, Colorado, 1966), Vol. VIIIC; G. R. Satchler, Nucl. Phys. 55, 1 (1964).

[21]*Handbook of Mathematical Functions*, edited by M. Abramowitz and I. A. Stegun, National Bureau of Standards, Applied Mathematics Series No. 55 (U.S. GPO, Washington, D. C., 1967).

[22]E. T. Copson, *Asymptotic Expansions* (Cambridge U. P., Cambridge, England, 1965).

[23]K. Alder, A. Bohr, T. Huus, B. Mottelson, and A. Winther, Rev. Mod. Phys. 28, 432 (1956).

[24]L. C. Biedenharn, J. L. McHale, and R. M. Thaler, Phys. Rev. 100, 376 (1955).

[25]C. M. Perey and F. G. Perey, Phys. Rev. 132, 755 (1963).

[26]S. A. Hjorth, E. K. Lin, and A. Johnson, Nucl. Phys. A116, 1 (1968).

[27]F. G. Perey, Phys. Rev. 131, 745 (1963).

[28]C. M. Vincent and H. T. Fortune, Phys. Rev. C 2, 782 (1970).